# **DEIO: Deep Event Inertial Odometry**

Weipeng Guan\*, Fuling Lin\*, Peiyu Chen, Peng Lu

Abstract-Event cameras are bio-inspired, motion-activated sensors that demonstrate impressive potential in handling challenging situations, such as motion blur and high-dynamic range. Despite their promise, existing event-based simultaneous localization and mapping (SLAM) approaches exhibit limited performance in real-world applications. On the other hand, state-of-the-art SLAM approaches that incorporate deep neural networks for better robustness and applicability. However, these is a lack of research in fusing learning-based event SLAM methods with IMU, which could be indispensable to push the event-based SLAM to large-scale, low-texture or complex scenarios. In this paper, we propose DEIO, the first monocular deep event-inertial odometry framework that combines learning-based method with traditional nonlinear graph-based optimization. Specifically, we tightly integrate a trainable eventbased differentiable bundle adjustment (e-DBA) with the IMU pre-integration in a factor graph which employs keyframebased sliding window optimization. Numerical Experiments in nine public challenge datasets show that our method can achieve superior performance compared with the image-based and event-based benchmarks. The source code is available at: https://github.com/arclab-hku/DEIO.

Index Terms—Event-based Vision, 6-DoF Pose Tracking, Event Camera, SLAM, Deep Learning, Robotics.

# I. INTRODUCTION

#### A. Motivation

CHIEVING reliable and accurate Simultaneous Localization and Mapping (SLAM) under adverse conditions remains challenging, particularly when employing image-based solutions (RGB or RGB-D cameras). Event camera is a motion-activated sensor that only captures pixelwise intensity changes and reports them as asynchronous stream instead of the whole scene at intensity image as a frame. Because of their remarkable properties, such as high temporal resolutions, high dynamic range (HDR), and no motion blur, event cameras have the potential to enable highquality perception in extreme lighting conditions and highspeed motion scenarios that are currently not accessible to standard cameras. Nevertheless, integrating event cameras into SLAM systems presents significant challenges. This is caused by the fact that the event data is sparse, irregular, and asynchronous, with each event conveying limited information and containing inherent noise. What's more, unlike standard-vision counterparts, event camera cannot capture visual information when motion is parallel to edges or in

This work was supported by General Research Fund under Grant 17204222, and in part by the Seed Fund for Collaborative Research and General Funding Scheme-HKU-TCL Joint Research Center for Artificial Intelligence.

static state. Therefore, current purely event-based SLAM systems [1], [2] generally lack the robustness requirement for many real-world applications.

Using additional sensors tends to achieve superior performance since different modalities can complement each other, such as image frame [3]–[5], depth sensors [6], or even LiDAR [7]. However, these combination might limit the application of event cameras in real-world devices due to increased costs and more complicated sensor calibration requirements [8]. What's more, they might introduce some bottlenecks, for example, relying the image frames might makes the system susceptible to motion blur and reduce the benefits of HDR.

Recent studies have introduced learning-based approaches [9] as promising solutions for event-based SLAM. These methods, which are solely trained end-to-end on synthetic events, demonstrate remarkable generalization to real-world benchmarks and can outperform some traditional systems in accuracy. However, it's important to note that visual-only systems have inherent limitations, making them vulnerable to low-textured environments and suffering from scale ambiguity. To address these visual degradation, a promising strategy is to incorporate multiple sensors, the Inertial Measurement Unit (IMU), which is low-cost and readily available in most event cameras. What's more, in the minimal configuration of a monocular setup, the IMU can also be used to recover the metric scale and provide higher accurate and more robust system. Despite this promising, learning-based event SLAM with IMU remains an unexplored territory.

# B. Contributions

Therefore, in this paper, we propose a deep learning-based event-inertial odometry (DEIO), which combines learningbased methods with traditional nonlinear graph-based optimization. We leverage the strengths of neural networks in predicting event correspondence, replacing the optical flow or hand-craft event-corner feature tracking [10]. To the best of our knowledge, DEIO is the first learning-based eventinertial odometry framework. More specifically, we design the learning-optimization-combined framework that tightlycoupled integrate trainable event-based differentiable bundle adjustment (e-DBA) with IMU pre-integration. In the framework, event-based recurrent optical flow and e-DBA are performed among consecutive event streams. The Hessian information is derived from e-DBA and further fed into a generic factor graph, facilitating integration with the IMU through keyframe-based sliding window optimization. The e-DBA is trained on synthetic event data but demonstrate

<sup>\*</sup>Equal contribution;

The authors are with the Adaptive Robotic Controls Lab (ArcLab), Department of Mechanical Engineering, The University of Hong Kong, Hong Kong SAR, China. (corresponding author: lupeng@hku.hk).

strong generalization on real-world challenge scenarios. Our main contributions can be summarized as follows:

- We propose a learning-based event-inertial odometry, which integrates a trainable e-DBA and IMU information through graph-based optimization, which improves the accuracy and robustness of pose estimation.
- 2) DEIO is the first learning-based monocular eventinertial odometry. Even though training on synthetic data, it outperforms over 20 state-of-the-art methods across 9 challenging real-world event benchmarks. The performance gap is further increased when trained on real data.
- We release our code and the preprocessed event data to facilitate further research in learning-based event pose tracking.

#### II. RELATED WORK

## A. Traditional Approaches for Event-based SLAM

The first purely event-based VO was presented in [11], which performed real-time event-based SLAM through three decoupled probabilistic filters that jointly estimate the 6-DoF camera pose, 3D map of the scene, and image intensity. However, it is computationally expensive and requires GPU to achieve real-time performance. EVO [1] presents a geometric 2D-3D model alignment, utilizing the 2D imagelike event representation and the 3D map reconstructed from EMVS [12]. It can perform on small-scale scenes, but it is highly parameter-sensitive and requires to run in the scene that is planar to the sensor, up to several seconds, for bootstrapping the system. ESVO [2] is the first stereo eventbased VO method to estimate the ego motion through the 2D-3D edge registration on time surface. However, it barely operates in real-time in low resolution event camera and also faces limitations due to rigorous initialization as well as unreliable pose tracking. What's more, some approaches reply on a pre-build photometric 3D map [13] or restrict the motion type to rotation-only [14]. However, most of them are prone to failure in challenging scenarios (such as fast motion), which negates the unique advantages of event cameras.

To enhance the robustness of purely event-based VO, existing event-based SLAM methods have demonstrated good performance by incorporating additional sensors. Notably, event-inertial integration is a widely used approach to address the limitations of event-only SLAM, which provides scale awareness and continuity of estimation with minimal setup requirements. A monocular event-inertial odometry (EIO) is presented in [10], which employs the event-corner features with IMU measurement to deliver real-time and accurate 6-DoF state estimation. What's more, this EIO framework can provide good global consistency through loop closure of the event-based representation. Ultimate-SLAM [3] and PL-EVIO [4] investigate the complementary nature of events and images to present an event-image-IMU odometry (EVIO). Chamorro et al. [15] integrate the event-based line feature with the IMU to achieve high ultra-fast pose estimation. ESVIO [16] proposed the first stereo EIO and EVIO framework to estimate states through temporally and spatially event-corner feature association. EVI-SAM [17] introduced the first event-based hybrid pose tracking framework, merging the feature-based and direct-based methods. Additionally, it consistently delivers excellent mapping results in a variety of challenging scenarios, demonstrating performance comparable to learning-based and NeRF-based mapping methods. Despite such remarkable success, current event-based SLAM systems still fall short of the robustness required for certain real-world applications, and their performance has hit a bottleneck, this directs toward the exploration of deep learning approaches.

## B. Learning-based Approaches for Event-based SLAM

Zhu et al. [18] constructed a convolutional neural networks (CNN) with an unsupervised encoder-decoder architecture for semi-dense depth prediction. Hidalgo-Carrió et al. [19] was the first to estimate dense depth maps from a monocular event camera through recurrent CNN architecture. Gehrig et al. [20] apply recurrent neural networks (RNN) architecture which maintained an internal state that was updated through asynchronous events or irregular images and could be queried to dense depth estimation at any timestamp. Ahmed et al. [21] developed a deep event stereo network that reconstructs spatial image features from embedded event data and leverages the event features using the reconstructed image features to compute dense disparity maps. However, all of these methods require knowledge of camera motion and show poor generalization beyond the training scenarios.

DH-PTAM [22] proposed a stereo event-image parallel tracking and mapping system that replacing hand-crafted features with learned features. Klenk, et al. [9] extends the DPVO [23] to accommodate the event modality through voxel-based representation, which are able to demonstrate generalization from simulation to several real-world eventbased benchmarks. It shows good performance compared to both classical and deep-learning baselines. However, their results reveal a significant scale loss/ambiguity, and they requires the careful selection of the input data. Pellerito, et al. [24] introduces an end-to-end VO which also builds upon DPVO using complicated feature encoders to fuse asynchronous events with image data. However, it requires a minimum of 1.2 million events between each pair of frames and discards additional frames if this requirement is not met. More importantly, it failed to evaluate their methods under fast motion or HDR scenes, and could only operate in very limited amount of real event data without challenging situations.

Our framework is closely related to [9], [23] but extends these works by integrating trainable event representations with IMU through our learning-optimization-combined strategy to improve the performance and robustness. Additionally, it is important to note that a visual-only (event-only) system, such as DPVO [23] and DEVO [9] has inherent limitations, failures can manifest in numerous ways, such as in low-texture environment, divergence in the optimization

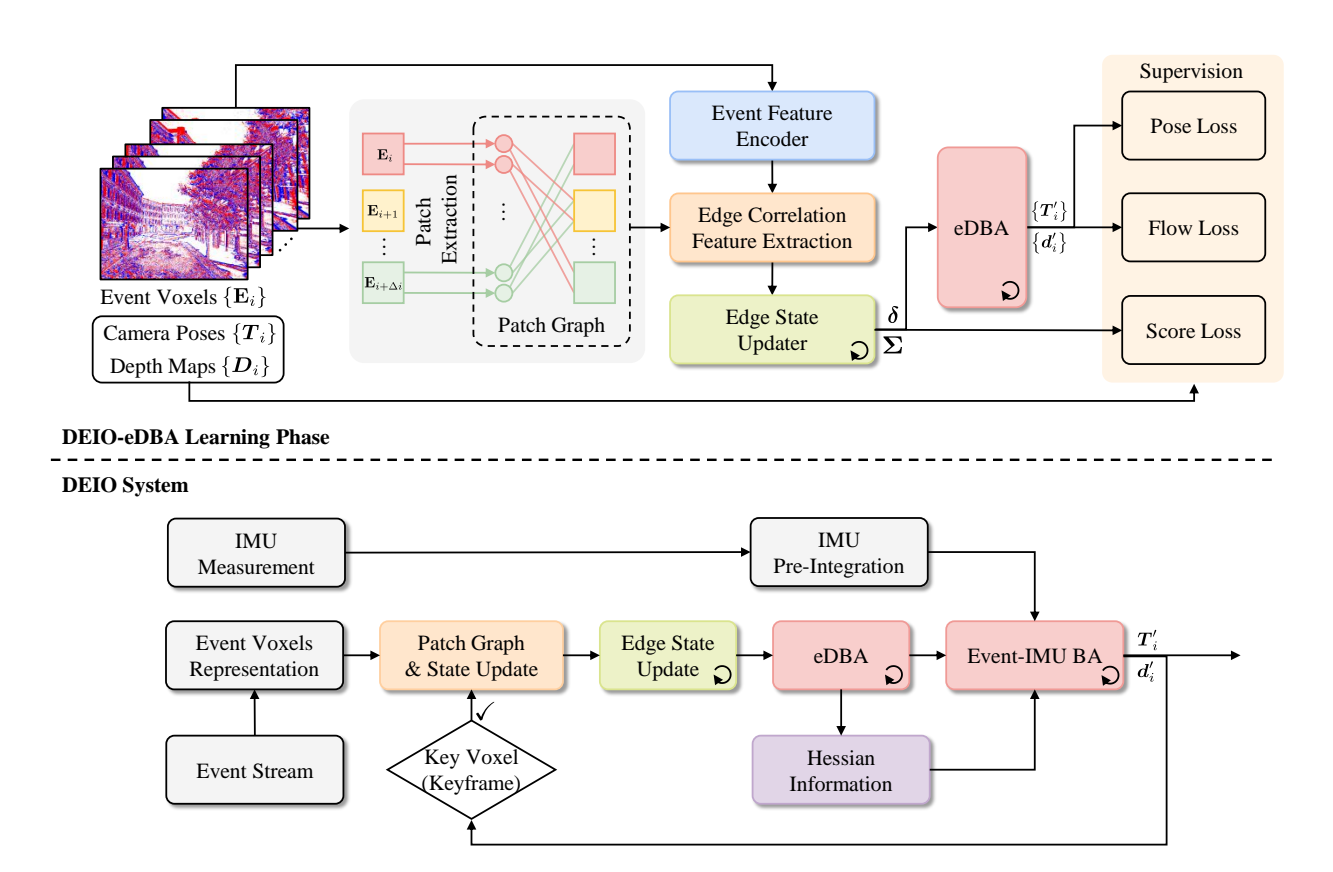


Fig. 1. Overview of the DEIO system. Our system builds upon the event-based recurrent optical flow network from [9], [23], and introduces a learning-optimization combined framework to enhance robustness and accuracy of state estimation. It utilizes a patch-based co-visibility factor graph to tightly-coupled fuse the Hessian information from the e-DBA and the IMU pre-integration using event-IMU combined bundle adjustment.

algorithm, scale ambiguity, and etc. Nevertheless, there is a absence of an implementation that incorporates learningbased event SLAM with IMU fusion framework.

## III. METHODOLOGY

The overall design of the framework aims to tightly-couple fuse the trainable eDBA with IMU pre-integration through optimization in a keyframe-based sliding window. Fig. 1 depicts the overview of our system. The main innovations of this work reside in how learning-based methods and traditional graph optimization are fused together. For the front-end, a deep neural network (Section III-A) is utilized to compute sparse patch-based correspondence for event-based recurrent optical flow. On the back-end, the reprojections are used to formulate an e-DBA problem, while the Hessian information derived from the e-DBA (detailed in Section III-C) is then tightly fused with the IMU preintegration through a patch-based co-visibility factor graph (Section III-D).

#### A. Network Structure for Event-based Optical Flow

In our framework, the event-based optical flow leverages the patch graph and recurrent network architecture from DPVO [23], which is a sparse patch-based VO derived from well-developed optical flow network (RAFT [25]). Additionally, we incorporate the voxel-based event representation

from [9] to effectively integrate the event modality into the DPVO. Each event voxel grid represents a frame-like structure of the event stream. The structure of the eventbased recurrent network is designed to estimate the 2D motion of the event patches across time by predicting optical flow. While the estimated optical flow is integrated into the differentiable bundle adjustment layer to update the depth of the event-patches and the camera poses. The structure for estimating event-patch trajectory consists of three primary components: (i) The CNN network that extracts patch-based event feature representations, capturing local context through matching and contextual features; (ii) The correlation layer that computes visual similarity between these event patches; (iii) The recurrent update operator that handles these eventpatches correspondence coupled with differentiable bundle adjustment. These construct the e-DBA problem, enabling end-to-end learning of reliable event-based optical flow, and optimize pose as well as depth of each patch iteratively through a differentiable bundle adjustment layer by minimizing the re-projection residual. The learning phase of Fig. 1 illustrates the complete process.

By dividing the event stream between frame i-1 and i into d equally spaced time intervals and aggregating each interval, an event voxel grid  $\mathbf{E}_i \in \mathbb{R}^{d \times H \times W}$  is obtained. After that, sparse event-patches are extracted to build the patch graph for scene representation. We denote the event

patches for frame i contains a series of  $P_{in}$  with size of  $p \times p$ :

$$m{P}_{in} = egin{bmatrix} m{x}_i \ m{y}_i \ 1 \ d_i \end{bmatrix} \quad m{x}_i, m{y}_i, m{d}_i \in \mathbb{R}^{1 imes p^2}$$

where  $d_i$  is the estimated inverse depth, assuming a constant depth for each individual event patch. The depth of each event patch is initialized using the median depth of all patches extracted from the previous three frames and would be further optimized in the e-DBA layer. We denote the  $n^{th}$  event patches for frame i as  $P_{in}$  with totally patch number N (N=96 in our implementations). Given the camera pose  $T_i$  in frame i, the camera intrinsics  $\pi$ , the event patch can be re-projected to other frame j and reconstruct the edges from  $P_{in}$  as (n,j), the edge-based patch graph  $\mathcal{G}$ . Thus the optimized pose  $T_{ij}$  and depth  $d_i$  can be obtain by minimizing the following cost function:

$$e = \sum_{i} \sum_{(n,j) \in \mathcal{G}} ||F(T_{ij}, d_i)||_{\Sigma_{inj}}^{2}$$

$$= \sum_{i} \sum_{(n,j) \in \mathcal{G}} ||\pi[T_{j}^{-1} \cdot T_{i} \cdot \pi^{-1}(\hat{P}_{in})] - [\hat{P}_{in} + \delta_{inj}]||_{\Sigma_{inj}}^{2}$$
(2)

where  $\pi$  and  $\pi^{-1}$  is the projection and back-projection function of the event camera.  $(\delta_{inj}, \Sigma_{inj})$  is the patch-based optical flow field predicted by the event-based recurrent network. The term  $\delta_{inj} \in \mathbb{R}^2$  denotes a 2D flow vector that indicates how the re-projection of the event-patch center should be updated, while the  $\Sigma_{inj}$  serves as the patchwise confidence weight of the optical flow.  $\hat{\mathbf{P}}_{in}$  denotes the center of the patch  $\mathbf{P}_{in}$ .  $T_i$  and  $T_j$  is the event camera pose in  $\mathbb{SE}(3)$ . Outlier rejection is handled automatically by the network, enhancing robustness compared to classical event-based SLAM systems.

# B. Training and Supervision for the e-DBA

The learning process for e-DBA of DEIO leverages supervision from poses, flow, and patch selection scores. The pose loss,  $\mathcal{L}_{pose}$ , is calculated as follows:

$$\mathcal{L}_{\text{pose}} = \sum_{i=1}^{N} \left\| \log_{\mathbb{SE}(3)} (T_{\text{GT},ij}^{-1} T_{ij}^{'}) \right\|$$
(3)

where  $T_{\text{GT},ij}$  and  $T_{ij}^{'}$  are the ground truth and updated poses of e-DBA between timestamp i and j respectively ( $T_{ij}^{'} = T_{i}^{-1}T_{j}^{'}$ ). The flow loss,  $\mathcal{L}_{\text{flow}}$ , measures the average distance between the estimated and ground truth optical flow over edges in the patch graph, where the frame distance between the source and target frames of each event-patch is within two frames. Regarding the event-patch selection, given the sparsity of event data in voxel, to avoid selecting event-patch from event-free regions, we follow [9] by adopting a patch selection network to propose regions for patch extraction and the loss on selection scores  $\mathcal{L}_{\text{score}}$ . The overall loss is then defined as a weighted combination:  $\mathcal{L} = 10\mathcal{L}_{\text{pose}} + 0.1\mathcal{L}_{\text{flow}} + 0.05\mathcal{L}_{\text{score}}$ .

The e-DBA is implemented in PyTorch and trained for 240K steps on two NVIDIA RTX-3090 GPUs. Each step uses a batch size of 1 with a sequence of 15 frames where the first 8 frames are used for initialization, and the remaining 7 frames are incrementally added for training. During training, each frame contains 80 event patches, each sized 12px×12px. In the first 1000 training steps, the network estimates only the depth of patches with fixed poses, allowing it to stabilize early training. In the subsequent steps, it jointly estimates both pose and patch depth. In the edge state updater, we conduct 18 iterations, supervising the pose and flow at each iteration, while the selection score is supervised only in the final iteration. Regarding the optimization objective Eq. 2 in e-DBA, we perform two Gauss-Newton iterations to refine poses and patch depths, ensuring that the predicted flow aligns with the camera motion.

Since the recurrent optical flow pipeline has demonstrated strong generalization [9], [23], [25], [26], we utilize the network weights pre-trained on the synthetic event-based TartanAir [27] dataset using the ESIM [28] simulator for all subsequent tests in this work. To further bridge the sim-to-real gap, we fine-tune the pre-trained model by incorporating real data into the training process. The resulting performance improvements would be further discussed in Section IV-D

# C. Hessian Derived from the e-DBA

The linearized expression of the re-projection errors in Eq. (2) can be written as:

$$\delta F(T_{ij}, d_i) = \begin{bmatrix} J_{ij} & J_{d_i} \end{bmatrix} \begin{bmatrix} \xi_{ij} \\ \Delta d_i \end{bmatrix}$$
(4)

where  $\delta F(T_{ij}, d_i) \in \mathbb{R}^2$  is the residual matrix with size of  $2NK \times 1$ . The  $\xi_{ij}$  is the Lie algebras of the updated pose  $T_{ij}$  in  $\mathfrak{se}(3)$ .  $\Delta d_i$  denotes the error state of the inverse depth. The Jacobians  $J_{ij}, J_{d_i}$  are with respect to the update pose  $T_{ij}$  and depth  $\Delta d_i$ , respectively. An event-patch  $P_{in}$  can be re-projected from frame i into frame j follows the warping function:

$$\mathbf{P}_{jn}^{'} = \begin{bmatrix} x_j & y_j & z_j & w_j \end{bmatrix}^T = \pi [\mathbf{T}_j^{-1} \cdot \mathbf{T}_i \cdot \boldsymbol{\pi}^{-1} (\hat{\mathbf{P}}_{in})]$$
 (5)

Thereofre, the Jacobians of the re-projection can be expressed as:

$$\mathbf{J}_{ij} = \begin{bmatrix} \frac{f_x w_j}{z_j} & 0 & -\frac{f_x x_j w_j}{z_j^2} & -\frac{f_x x_j y_j}{z_j^2} & f_x + \frac{f_x x_j^2}{z_j^2} & -\frac{f_x y_j}{z_j^2} \\ 0 & \frac{f_y w_j}{z_j} & -\frac{f_y y_j w_j}{z_j^2} & -f_y - \frac{f_y y_j^2}{z_j^2} & \frac{f_y x_j y_j}{z_j^2} & -\frac{f_y x_j}{z_j^2} \end{bmatrix}$$
(6)

where  $f_x$  and  $f_y$  are the given event camera intrinsic parameters. While the  $J_{d_i}$  can be given as:

$$J_{d_i} = \begin{bmatrix} f_x(\frac{t_{ij}[0]}{z_j} - \frac{t_{ij}[2]x_j}{z_j^2}) \\ f_y(\frac{t_{ij}[1]}{z_j} - \frac{t_{ij}[2]y_j}{z_j^2}) \end{bmatrix}$$
(7)

where the  $t_{ij}$  is the translation vector of the related transform between  $T_i$  and  $T_j$ . Then, the Hessian Matrix of Eq. (2) can be computed following:

By decoupling the pose and depth variables, the system can be efficiently solved using the Schur complement:

$$H\begin{bmatrix} \boldsymbol{\xi}_{ij} \\ \Delta \boldsymbol{d}_{i} \end{bmatrix} = -\begin{bmatrix} \boldsymbol{J}_{ij} & \boldsymbol{J}_{\boldsymbol{d}_{i}} \end{bmatrix}^{T} \boldsymbol{W} \boldsymbol{F}(\boldsymbol{T}_{ij}, \boldsymbol{d}_{i})$$

$$\begin{bmatrix} \boldsymbol{B} & \boldsymbol{E} \\ \boldsymbol{E}^{T} & \boldsymbol{C} \end{bmatrix} \begin{bmatrix} \boldsymbol{\xi}_{ij} \\ \Delta \boldsymbol{d}_{i} \end{bmatrix} = \begin{bmatrix} \boldsymbol{v} \\ \boldsymbol{u} \end{bmatrix}$$
(9)

and leading to the following equation:

$$\boldsymbol{\xi_{ij}} = \underbrace{[\boldsymbol{B} - \boldsymbol{E}\boldsymbol{C}^{-1}\boldsymbol{E}^T]^{-1}}_{\boldsymbol{Haa}}\underbrace{(\boldsymbol{v} - \boldsymbol{E}\boldsymbol{C}^{-1}\boldsymbol{u})}_{\boldsymbol{Vaa}}$$
(10)

where  $\boldsymbol{v}$  is a  $6 \cdot K \times 1$  vector (with 6 DoF pose and totally K=10 keyframe), and  $\boldsymbol{u}$  is an  $N \cdot K \times 1$  vector (with totally number of N=96 event patches for each frame). The  $\boldsymbol{B}$  is the matrix with size of  $60 \times 60$ ,  $\boldsymbol{E}$  is the residual matrix with size of  $60 \times 960$ , and  $\boldsymbol{C}$  is a diagonal matrix with size of  $960 \times 960$ . A damping factor of  $10^{-4}$  is also applied to  $\boldsymbol{C}$  as [23]. These matrices establish an inter-frame pose constraint (represented by  $\boldsymbol{Hgg}$  and  $\boldsymbol{Vgg}$ ) that integrates the e-DBA information. After updating the camera poses  $\boldsymbol{T}_j' = \boldsymbol{T}_i \cdot \boldsymbol{T}_{ij}'$ ,  $\boldsymbol{T}_{ij} = exp(\boldsymbol{\xi_{ij}})$ , the inverse depth of each event patch would be updated as:

$$d'_{i} = \Delta d_{i} + d_{i}$$

$$\Delta d_{i} = C^{-1}(u - E^{T} \xi_{ij})$$
(11)

The calculations of Eq. (10) and Eq. (11) can be efficiently performed in parallel on GPU with CUDA acceleration. While all the Hessian information Hgg and the corresponding Vgg, derived from the co-visibility graph, are integrated into the factor graph where they are optimized on the CPU. The e-DBA contributes extensive geometric information, incorporating learned uncertainties, to the factor graph. While the optimization results (updated poses and depths) are then iteratively fed back to refine/re-weight the event-based optical flow network. This recurrent process enhances the robustness and accuracy of the overall system.

## D. Graph-based e-DBA and IMU Optimization

Unlike end-to-end approaches that use networks to fuse the features from two modalities (event and IMU) and predict poses directly, our DEIO combine the neural networks with event-inertial bundle adjustment. To this end, we design a learning-optimization-combined framework that tightly-coupled integrate the Hessian information from e-DBA and IMU pre-integration within keyframe-based sliding window optimization. The full state vector in the sliding window, with k (total number of keyframes K=10 in our implementation), is defined as:

$$\chi = [T_{b_k}^w, v_{b_k}^w, b_{a_k}, b_{g_k}], k = 1, 2, 3, ...$$
(12)

where  $\boldsymbol{T}_{b_k}^w = \begin{bmatrix} \boldsymbol{R}_{b_k}^w & \boldsymbol{t}_{b_k}^w \\ 0 & 1 \end{bmatrix} \in \mathbb{SE}(3)$  is the pose of the body (IMU) frame in the world frame, given by the translation  $\boldsymbol{t}_{b_k}^w$  and rotation matrix  $\boldsymbol{R}_{b_k}^w$ ;  $\boldsymbol{v}_{b_k}^w$  is the velocity of the IMU in the world frame;  $\boldsymbol{b}_{a_k}$  and  $\boldsymbol{b}_{g_k}$  is the accelerometer bias and gyroscope bias, respectively.

We solve the state estimation problem by constructing a factor graph with the GTSAM library and optimizing it with the Levenberg-Marquardt. The cost function, which minimizes residuals from various factors corresponding to different aspects of data constraints, can be written as:

$$J(\chi) = ||r_{event}^k||_{W_{event}^k}^2 + \sum_{k=0}^{K-1} ||r_{imu}^k||_{W_{imu}^k}^2 + ||r_m||_{W_m}^2$$
(13)

Eq.(13) contains the event-based residuals  $r_{event}^k$  with weight  $W_{event}^k$ ; the IMU pre-integration residuals  $r_{imu}^k$  with weight  $W_{imu}^k$ ; the marginalization residuals  $r_m$  with weight  $W_m$ :

Given the Hessian information Hgg and the corresponding Vgg, the event residual factor can be written like [29]:

$$r_{event}^{k} = \frac{1}{2} \begin{bmatrix} \boldsymbol{\xi}_{e_0}^{w} & \boldsymbol{\xi}_{e_1}^{w} & \cdots & \boldsymbol{\xi}_{e_k}^{w} \end{bmatrix} \boldsymbol{H} \boldsymbol{g} \boldsymbol{g} \begin{bmatrix} \boldsymbol{\xi}_{e_0}^{w} \\ \boldsymbol{\xi}_{e_1}^{w} \\ \vdots \\ \boldsymbol{\xi}_{e_k}^{w} \end{bmatrix} - \begin{bmatrix} \boldsymbol{\xi}_{e_0}^{w} & \boldsymbol{\xi}_{e_1}^{w} & \cdots & \boldsymbol{\xi}_{e_k}^{w} \end{bmatrix} \boldsymbol{V} \boldsymbol{g} \boldsymbol{g}$$

$$(14)$$

where  $\boldsymbol{\xi}^w_{e_k} = \boldsymbol{\xi}^e_b \cdot \boldsymbol{\xi}^w_{b_k}$ , and  $\boldsymbol{\xi}^w_{b_k} = \log_{\mathbb{SE}(3)}(\boldsymbol{T}^w_{b_k})$ . While  $\boldsymbol{\xi}^w_{e_k}$  and  $\boldsymbol{\xi}^w_{b_k}$  are the Lie algebras of the event camera pose and IMU pose in  $k^{th}$  keyframe, respectively.  $\boldsymbol{\xi}^e_b$  is the extrinsics of the event camera and IMU.

Eventually, the IMU residual factor can be derived as follows:

$$\boldsymbol{r}_{imu}^{k} = \begin{bmatrix} \boldsymbol{R}_{w}^{b_{k}} (\boldsymbol{t}_{b_{k+1}}^{w} - \boldsymbol{t}_{b_{k}}^{w} - \boldsymbol{v}_{b_{k}}^{w} \Delta t - \frac{1}{2} \boldsymbol{g}^{w} \Delta t^{2}) - \hat{\boldsymbol{\alpha}}_{b_{k+1}}^{b_{k}} \\ \boldsymbol{R}_{w}^{b_{k}} (\boldsymbol{v}_{b_{k+1}}^{w} - \boldsymbol{v}_{b_{k}}^{w} - \boldsymbol{g}^{w} \Delta t) - \hat{\boldsymbol{\beta}}_{b_{k+1}}^{b_{k}} \\ 2 \left[ (\boldsymbol{q}_{b_{k}}^{w})^{-1} \otimes \boldsymbol{q}_{b_{k+1}}^{w} \otimes (\hat{\boldsymbol{\gamma}}_{b_{k+1}}^{b_{k}})^{-1} \right]_{xyz} \\ \boldsymbol{b}_{a_{k+1}} - \boldsymbol{b}_{a_{k}} \\ \boldsymbol{b}_{g_{k+1}} - \boldsymbol{b}_{g_{k}} \end{bmatrix}$$

$$(15)$$

where  $\alpha_{b_{k+1}}^{b_k}$ ,  $\beta_{b_{k+1}}^{b_k}$ ,  $\gamma_{b_{k+1}}^{b_k}$  are the IMU pre-integration term [4];  $\boldsymbol{g}^w$  is the gravity vector;  $\Delta t$  is the time interval between keyframe k and k+1;  $\boldsymbol{q}_w^{b_k}$  is the quaternion of the corresponding rotation matrix  $\boldsymbol{R}_w^{b_k}$  with  $[\cdot]_{xyz}$  extracts the vector portion.

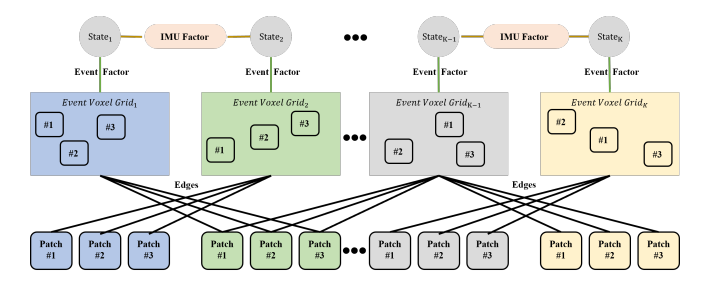


Fig. 2. Patch-based co-visibility factor graph

# E. EIO System

As illustrated in Fig. 2, our DEIO maintains a patch-based co-visibility factor graph that takes the raw event stream and IMU data as input, and perform 6 DoF pose estimation.

Initialization: We use 8 frames for event-only initialization. The new event patches are added until 8 frames are accumulated, and then run 12 iterations of the update operator, followed by two event-only bundle adjustment iterations. Since the IMU provides scale awareness and the gravity direction, it is essential to initialize the states in a metric-scale local frame for better convergence. Similar to the initialization procedure from [30], [31], where the visiononly structure from motion (SfM) is replaced by the eventonly bundle adjustment, after the event-only initialization, we further employ the IMU pre-integration to establish the up-to-scale camera pose. After linear alignment and gravity refinement, the scale between IMU and event camera is restored, with further correction applied to the depth of the event-based patch. Subsequently, the event-IMU bundle adjustment (Section III-D) is iteratively performed by updating the co-visibility graph based on the event-inertial initialization results. To enable initialization, enough camera motion is required. During the event-only initialization, we accumulate only frames that exhibit an average optical flow magnitude of at least 8 pixels (estimated by performing one update iteration) from the prior frame. What's more, sufficient excitation is also required from the IMU, with the gyroscope's variance exceeding 0.25.

Co-visibility Patch Graph Management: When a new event patch is added, the edges between that event patch and the previous r keyframes (r=13 in our implementations) are added into the patch graph. After appending these new edges (with the predicted event-based optical flow field  $(\delta_{inj}, \Sigma_{inj})$ ), the update operation of the patch graph is performed, including recurrent update operator and the 2 event-IMU bundle adjustment iterations. After that, the keyframe selection is perform to maintain the keyframe-based sliding window.

**Keyframe Strategy:** The most recent 3 frames are always considered as keyframes. After each update operation of the co-visible graph, the optical flow magnitude between the  $(t-5)^{th}$  and  $(t-3)^{th}$  keyframe would be calculated. If this magnitude is less than 60 pixels, the  $(t-4)^{th}$  keyframe, along with all associated edges and patch-based features, would be removed. Additionally, the event patches and keyframe are discarded once they fall outside the optimization window. The oldest keyframe that is abandoned would be marginalized, along with its associated IMU preintegration, to construct the marginalization factor  $r_m$  in Eq. (13).

## IV. EXPERIMENTS

We conducted quantitative and qualitative evaluations of our DEIO across *nine* challenging real-world datasets with varying camera resolution and diversity scenarios on different platforms. Specifically, in subsections IV-B and IV-C, we assess the performance of our DEIO in night driving scenarios and indoor low-light quadrotor flights, respectively. DEIO is compared against over 20 baseline methods from various literature, including both event-based and imagebased approaches. Additionally, we proposed three additional baselines: (i) DPVO [23], which operates on the

RGB frames of the respective dataset; (ii) DBA-Fusion [29], a learning-based VIO framework that combines DROID-SLAM [26] with IMU data, which runs on the RGB frames and IMU; (iii) a modified version of our proposed learning-optimization-combined framework that uses images and IMU data as inputs, referred to as DVIO<sup>†</sup>. It operates on the standard images and IMU data from the respective datasets, with the network weights provided by [23]. This enables a comparison between events and images within the same framework and parameters.

To ensure fair comparison, same trajectory alignment protocol is required, therefore, we had to employ different alignment ways and evaluation criterion according to the compared baseline methods. For example, regarding the DAVIS240c dataset [32], the estimated and ground-truth trajectories were aligned using a 6-DOF transformation (in SE3) over a 5-second interval [0-5s], and we calculated the mean position error (MPE) as a percentage of the total traveled distance of the ground truth as the evaluation criterion. In contrast, for the stereo HKU dataset [16], although MPE is also used as the metric, to maintain consistency with the baseline methods, we aligned the estimated trajectories and ground truth in SE3 using all available data rather than just the 5-second segment, While for the TUM-VIE dataset [33], the baseline methods calculated the root-meansquare (RMSE) of the Absolute Trajectory Errors (ATE) based on the estimated camera pose as the evaluation criterion. To avoid confusion, we would annotate the trajectory alignment protocol in the footnotes of each table, ensuring that different methods within the same table utilize the same alignment protocol. What's more, the notations E, F, and I in each table represent the use of event, frame, and IMU, respectively, which helps facilitate a better performance comparison among different modalities.

A. Comparison with SOTA Methods in Challenge Benchmarks

We only choose the challenge enough real-world event dataset for our evaluations, and the details of these benchmark evaluation are as follows:

**DAVIS240C** [32]: This is the most classical monocular event-based SLAM benchmark, which provides event and image data with a resolution of 240×180 pixels, as well as IMU data and 200HZ ground truth poses. It contains extremely fast 6-Dof motion and scenes with HDR. The estimated and ground-truth trajectories were aligned with a 6-DOF transformation (in SE3), using 5 seconds [0-5s] of the resulting trajectory. We computed the mean position error (MPE) as percentages of the total traveled distance of the ground truth, which are calculated by the publicly available trajectory evaluation tool [41].

The baseline results (except for DPVO, DBA-Fusion, DEVO, and DVIO $^{\dagger}$ ) are directly taken from the original works, which also employed the same trajectory alignment protocol. As can be seen from Table I, EVI-SAM achieved the best performance among the non-learning methods.

TABLE I. Accuracy Comparison of Our DEIO with Other Monocular Event-based Baseline in DAVIS240c Dataset [32]

Methods	Modality	boxes_translation	hdr_boxes	boxes_6dof	dynamic_translation	dynamic_6dof	poster_translation	hdr_poster	poster_6dof	Average
Zhu et al. [34]	E+I	2.69	1.23	3.61	1.90	4.07	0.94	2.63	3.56	2.58
Henri et al. [35]	E+I	0.57	0.92	0.69	0.47	0.54	0.89	0.59	0.82	0.69
Ultimate-SLAM [3]	E+I	0.76	0.67	0.44	0.59	0.38	0.15	0.49	0.30	0.47
Ollimate-SEAW [3]	E+F+I	0.27	0.37	0.30	0.18	0.19	0.12	0.31	0.28	0.25
Jung et al. [36]	E+I	1.50	2.45	2.88	4.92	6.23	3.43	2.38	2.53	3.92
Julig Ct al. [50]	E+F+I	1.24	1.15	0.98	0.89	0.98	1.83	0.57	0.97	1.07
HASTE-VIO [37]	E+I	2.55	1.75	2.03	1.32	0.52	1.34	0.57	1.50	1.45
EKLT-VIO [38]	E+F+I	0.48	0.46	0.84	0.40	0.79	0.35	0.65	0.35	0.54
Dai et al. [39]	E+I	1.0	1.8	1.5	0.9	1.5	1.9	2.8	1.2	1.56
Mono-EIO [10]	E+I	0.34	0.40	0.61	0.26	0.43	0.40	0.40	0.26	0.39
PL-EVIO [4]	E+F+I	0.06	0.10	0.21	0.24	0.48	0.54	0.12	0.14	0.24
Lee et al. [40]	E+F+I	0.74	0.69	0.77	0.71	0.86	0.28	0.52	0.59	0.65
EVI-SAM [17]	E+F+I	0.11	0.13	0.16	0.30	0.27	0.34	0.15	0.24	0.21
DPVO [23]	F	0.02	0.71	0.59	0.09	0.05	0.20	0.49	0.44	0.32
DBA-Fusion [29]	F+I	0.07	0.27	0.10	0.56	0.11	0.13	0.38	0.19	0.23
DEVO [9]	E	0.06	0.06	0.71	0.09	0.08	0.06	0.14	0.44	0.21
$DVIO^{\dagger}$	F+I	0.05	0.11	0.06	0.26	0.06	0.07	0.38	0.09	0.14
DEIO	E+I	0.07	0.09	0.05	0.06	0.04	0.04	0.06	0.08	0.06

Unit: MPE(%), 0.06 means the average error would be 0.06m for 100m motion; Aligning 5 seconds [0-5s] of the estimated trajectory with the ground truth;

TABLE II. Accuracy Comparison of Our DEIO with Other Image/Event-based Baseline in Mono-HKU Dataset [10]

Resolution	Methods	Modality	vicon _hdr1	vicon _hdr2	vicon _hdr3	vicon _hdr4	vicon _darktolight1	vicon _darktolight2	vicon _lighttodark1	vicon _lighttodark2	vicon _dark1	vicon _dark2	Average
	ORB-SLAM3 [42]	F	0.32	0.75	0.60	0.70	0.75	0.76	0.41	0.58	failed	0.60	0.61
	VINS-MONO [30]	F+I	0.96	1.60	2.28	1.40	0.51	0.98	0.55	0.55	0.88	0.52	1.02
	DPVO [23]	F	0.10	0.05	0.12	0.08	0.14	0.08	0.16	0.10	0.06	0.05	0.09
DBA-Fusion [29]	DBA-Fusion [29]	F+I	0.32	0.41	failed	failed	0.72	0.55	failed	2.65	3.32	failed	1.33
	Ultimate-SLAM [3]	E+I	1.49	1.28	0.66	1.84	1.33	1.48	1.79	1.32	1.75	1.10	1.40
DAVIS346	Offinate-SLAW [3]	E+F+I	2.44	1.11	0.83	1.49	1.00	0.79	0.84	1.49	3.45	0.63	1.41
(346*260)	Mono-EIO [10]	E+I	0.59	0.74	0.72	0.37	0.81	0.42	0.29	0.79	1.02	0.49	0.62
	PL-EIO [4]	E+I	0.57	0.54	0.69	0.32	0.66	0.51	0.33	0.53	0.35	0.38	0.49
	PL-EVIO [4]	F+E+I	0.17	0.12	0.19	0.11	0.14	0.12	0.13	0.16	0.43	0.47	0.20
	DEVO [9]	E	0.11	0.07	0.12	0.07	0.97	0.12	0.15	0.12	0.07	0.07	0.19
	DVIO <sup>†</sup>	F+I	0.10	0.18	0.31	0.17	0.15	0.14	0.14	0.26	0.07	0.35	0.19
	DEIO	E+I	0.14	0.09	0.16	0.07	0.11	0.10	0.11	0.13	0.05	0.08	0.10

Unit: MPE(%); Aligning 5 seconds [0-5s] of the estimated trajectory with the ground truth;

However, developed from the feature-based method (PL-EVIO) to the combined direct and feature-based method (EVI-SAM), it's evident that traditional methods have reached a performance bottleneck, as even the powerful EVI-SAM only offers marginal improvements. In contrast, learning-based methods (such as DEVO) can achieve performance comparable to EVI-SAM using purely event sensors, highlighting the effectiveness and strength of learning-based approaches. While our learning-optimization combined methods exhibits significantly superior performance compared to other learning-based methods (DPVO, DBA-FUsion,DEVO, DVIO†). Compared with DEVO, our proposed DEIO decrease the pose tracking error by up to 71%, thanks to the organic combination of learning and traditional optimization method.

Monocular HKU-dataset [10]: This dataset was collected using DAVIS346 (346 × 260, event, image, and IMU sensor), along with a motion capture system (VICON) to obtain pose ground truth. To mitigate the significant impact of the active infrared (IR) emitters from the VICON cameras on the event camera, an IR filter lens was used to eliminate IR interference. As a result, this dataset exhibits more serious thermal noise than others. Furthermore, all sequences were recorded in HDR scenarios under very low illumination or strong illumination changes by switching the strobe flash on and off. Table II demonstrates that DEIO outperform all the

event-based methods and decrease the average pose tracking error by at least 47%. Fig. 3(b) illustrates the estimated trajectory of our DEIO, which shows less drift compared to DEVO, verifying the contribution of IMU integration to maintain low-drifting, metric-scale pose estimation.

Stereo HKU-dataset [16]: This dataset contains stereo event data at 60Hz and stereo image frames at 30Hz with resolution in  $346 \times 260$ , as well as IMU data at 1000Hz. It consists of handheld sequences including rapid motion and HDR scenarios. In Table III, our method outperforms all previous works in terms of average positioning error. Moreover, DEIO beats the DEVO and increase the average accuracy of the sequences up to 48%, especially on  $agg\_walk$  and  $agg\_flip$ . DEVO encounters significant errors due to the limitations of relying solely on monocular event camera. As shown in Fig. 3(c), our trajectory aligns perfectly with the ground truth, while DEVO exhibits serious scale loss.

**VECtor** [45]: This dataset consists of a hardware-synchronized sensor suite that includes stereo event cameras  $(640 \times 480)$ , stereo standard cameras  $(1224 \times 1024)$ , and IMU. It covers the full spectrum of 6 DoF motion dynamics, environment complexities, and illumination conditions for both small and large-scale scenarios. As seen in Table IV, our proposed DEIO achieves outstanding results on average. It beats all image-based baselines with high-quality frames,

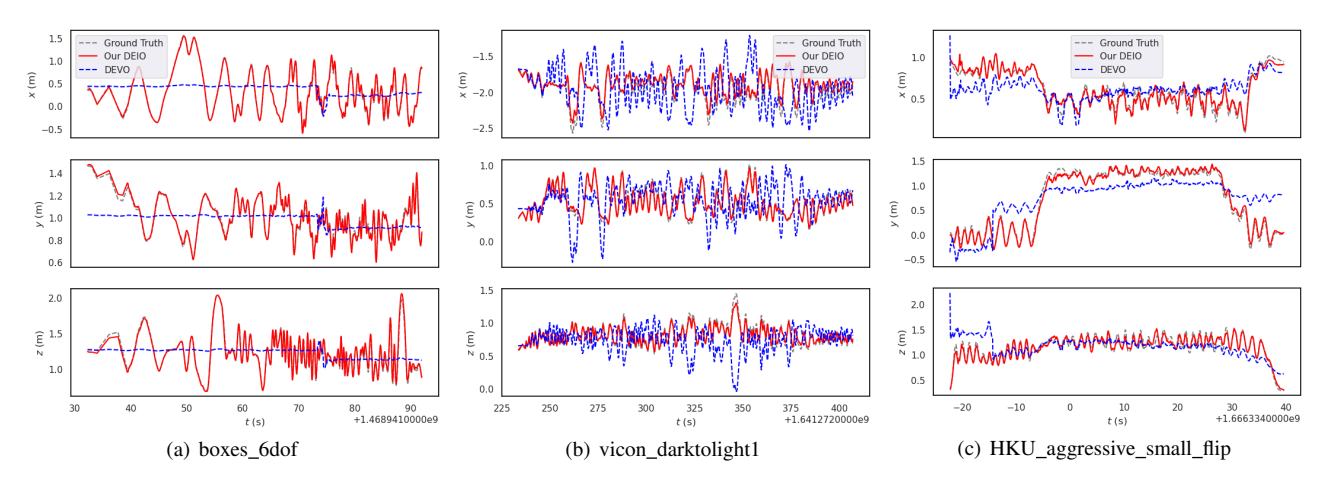


Fig. 3. Comparison of estimated trajectories on challenge sequences from [10], [16], [32].

TABLE III. Accuracy Comparison of Our DEIO with Other Image/Event-based Baseline in Stereo-HKU Dataset [16]

Methods	Modality	agg_translation	agg_rotation	agg_flip	agg_walk	hdr_circle	hdr_slow	hdr_tran_rota	hdr_agg	dark_normal	Average
ORB-SLAM3 [42]	Stereo F+I	0.15	0.35	0.36	failed	0.17	0.16	0.30	0.29	failed	0.25
VINS-Fusion [43]	Stereo F+I	0.11	1.34	1.16	failed	5.03	0.13	0.11	1.21	0.86	1.24
ESVO [2]	Stereo E	failed	failed	failed	failed	failed	failed	failed	failed	failed	_
EnVIO [44]	Stereo F+I	failed	2.12	2.94	3.38	0.85	0.43	0.37	0.50	failed	1.51
DPVO [23]	F	0.07	0.04	0.99	1.17	0.31	0.23	0.67	0.29	failed	0.47
DBA-Fusion [29]	F+I	0.13	0.16	0.83	0.37	0.18	failed	failed	0.10	0.27	0.29
PL-EVIO [4]	E+F+I	0.07	0.23	0.39	0.42	0.14	0.13	0.10	0.14	1.35	0.33
EVI-SAM [17]	E+F+I	0.17	0.24	0.32	0.26	0.13	0.11	0.11	0.10	0.85	0.25
ESIO [16]	Stereo E+I	0.55	0.78	3.17	1.30	0.46	0.31	0.91	1.41	0.35	1.03
ESVIO [16]	Stereo E+F+I	0.10	0.17	0.36	0.31	0.16	0.11	0.10	0.10	0.42	0.20
EVO [1]	E	failed	failed	failed	failed	failed	failed	failed	failed	failed	_
DEVO [9]	E	0.06	0.05	0.71	0.90	0.39	0.08	0.08	0.26	0.06	0.29
$\mathrm{DVIO}^{\dagger}$	F+I	0.05	0.06	0.19	1.33	0.15	0.08	0.07	0.04	0.12	0.23
DEIO	E+I	0.06	0.09	0.20	0.48	0.14	0.07	0.09	0.06	0.11	0.15

Unit: MPE(%); Aligning the whole ground truth trajectory with estimated poses; The notations E, F, and I stand for the use of event, frame, and IMU, respectively. The Baseline numbers (DPVO, DEVO) are taken from [9].

and even outperforms Ultimate-SLAM, PL-EVIO, ESVIO, and EVI-SAM on over 75% of the sequences, which utilize event, image and IMU. More Specifically, DEIO also performs better on average than DEVO on large-scale sequences thanks to the complementarity between event and IMU sensor. While the DEVO, monocular visual-only method encounters challenges in these low-texture scenes, and it is also limited by scale ambiguity and drift.

TUM-VIE [33]: This dataset was recorded with stereo high-resolution event cameras ( $1280 \times 720$ ) mounted on a helmet, capturing footage from an egocentric viewpoint. We evaluated our method on sequences recorded in a motion capture room that featured various 6DOF camera movements. The results can be seen in Table V. DEIO outperforms all previous works on four out of five sequences, even though DH-PTAM [22] utilizes four cameras of the setup (stereo events and stereo images).

UZH-FPV [47]: This dataset is a high-speed, aggressive dataset collected by monocular DAVIS346, which includes fast laps around a racetrack with drone racing gates, as well as free-form trajectories around obstacles. As shown in Table VI, this dataset is extremely challenging that even the most advanced learning-based VO (DPVO) fails on all sequences. However, our DEIO performed better than the baseline method on average. Indeed, the improvement

between DEIO and DEVO is not significant, which can be attributed to the serious IMU bias caused by aggressive motion. Consequently, the gains from the optimization with IMU are restricted. Nevertheless, our DEIO still successfully tracks long stretches of the flight involving to-fro motion, sudden change of direction and loops.

MVSEC [48]: This dataset is collected by stereo DAVIS346. Specifically, we selected the indoor\_flying sequence, which features arbitrary 6-DOF motion from a drone flying in a motion capture room. The rapid forward and backward movements of the drone, combined with hovering pauses that generate almost no events, make this scenario particularly challenging. Additionally, the few events generated far from the camera is further challenging event-based SLAM. In Table VII, we surpass the event-based baseline, especially, for the Flying\_4, we attain a RMSE of 40% lower than DEVO. However, due to the noisy event data of MVSEC, DEIO still performs worse than the learning-based VO (DPVO).

**DSEC** [49]: This dataset was collected with stereo event cameras  $(640 \times 480)$  mounted on a car driving through the streets of Switzerland. Since the DSEC dataset lacks ground truth trajectories, we used the odometry trajectories provided by [46] which is obtained through a LiDAR-IMU-based method, as ground truth. As can be seen from

TABLE IV. Accuracy Comparison of Our DEIO with Other Image/Event-based Baseline in Vector [45]

Methods	Modality	corner-	desk-	sofa-	mountain-	corridors-	corridors-	units-	units-	overe ac
Wiethous	Wiodanty	slow	normal	fast	fast	dolly	walk	dolly	scooter	average
ORB-SLAM3 [42]	Stereo F+I	1.49	0.46	0.21	2.11	1.03	1.32	7.64	6.22	2.81
VINS-Fusion [43]	Stereo F+I	1.61	0.47	0.57	failed	1.88	0.50	4.39	4.92	2.05
DPVO [23]	F	0.30	0.09	0.07	0.11	0.56	0.54	1.52	1.67	0.61
DBA-Fusion [29]	F+I	1.72	0.48	0.43	failed	1.37	0.59	1.23	0.48	0.90
EVO [1]	Е	4.33	failed	failed	failed	failed	failed	failed	failed	4.33
ESVO [2]	Stereo E	4.83	failed	failed	failed	failed	failed	failed	failed	4.83
Ultimate-SLAM [3]	E+F+I	4.83	2.24	2.54	4.13	failed	failed	failed	failed	3.44
PL-EVIO [4]	E+F+I	2.10	3.66	0.17	0.13	1.58	0.92	5.84	5.00	2.92
ESVIO [16]	Stereo E+F+I	1.49	0.61	0.17	0.16	1.13	0.43	3.43	2.85	1.41
EVI-SAM [17]	E+F+I	2.50	1.45	0.98	0.38	1.58	1.27	0.59	0.83	1.32
DEVO [9]	Е	0.59	0.11	0.38	0.37	0.51	1.04	0.48	0.88	0.55
$\mathrm{DVIO}^{\dagger}$	F+I	0.72	0.26	0.44	0.20	0.54	0.40	1.50	2.37	0.68
DEIO	E+I	0.50	0.13	0.44	0.24	0.78	0.74	0.35	0.35	0.44

Unit: MPE(%); Aligning the whole ground truth trajectory with estimated poses; The Baseline numbers (DPVO, DEVO) are taken from [9].

TABLE V. Accuracy Comparison of Our DEIO with Other Event-based Baseline in TUM-VIE [33]

Methods	Modality		Average					
wicthous	Wiodanty	1d-trans	3d-trans	6dof	desk	desk2	Average	
EVO [1]	Е	7.5	12.5	85.5	54.1	75.2	47.0	
ESVO [2]	Stereo E	12.3	17.2	13.0	12.4	4.6	11.9	
ES-PTAM [46]	Stereo E	1.05	8.53	10.25	2.5	7.2	5.9	
DH-PTAM [22]	Stereo E+F	10.3	0.7	2.4	1.6	1.5	3.9	
Ultimate-SLAM [3]	E+F+I	3.9	4.7	35.3	19.5	34.1	19.5	
DEVO [9]	E	0.5	1.1	1.6	1.7	1.0	1.2	
DEIO	E+I	0.4	1.1	1.4	1.4	0.7	1.0	

Unit:ATE/ RMSE(cm); Aligning the whole ground truth trajectory with estimated poses; The Baseline numbers (EVO, ESVO, and ES-PTAM) are taken from [46], while DH-PTAM and Ultimate-SLAM are sourced from [22], and DEVO is from [9].

TABLE VI. Accuracy Comparison of Our DEIO with Other Image/Event-based Baseline in UZH-FPV [47]

Methods	Modality		Average						
Wiethous	Modality	3	5	6	7	9	10	Average	
VINS-Fusion [43]	Stereo F+I	0.84	failed	1.45	0.61	2.87	4.48	2.45	
ORB-SLAM3 [42]	Stereo F+I	0.55	1.19	failed	0.36	0.77	1.02	0.78	
EVO [1]	E	failed	failed	failed	failed	failed	failed	_	
DPVO [23]	F	failed	failed	failed	failed	failed	failed	_	
VINS-MONO [30]	F+I	0.65	1.07	0.25	0.37	0.51	0.92	0.63	
DBA-Fusion [29]	F+I	failed	failed	failed	failed	failed	failed	_	
Ultimate SLAM [3]	E+F+I	failed	failed	failed	failed	failed	failed	_	
PL-EVIO [4]	E+F+I	0.38	0.90	0.30	0.55	0.44	1.06	0.60	
DEVO [9]	E	0.37	0.40	0.31	0.50	0.61	0.52	0.45	
$DVIO^{\dagger}$	F+I	failed	failed	failed	failed	failed	failed	_	
DEIO	E+I	0.39	0.36	0.33	0.32	0.59	0.55	0.42	

Unit: MPE(%); Aligning the whole ground truth trajectory with estimated poses; The Baseline numbers (DPVO, DEVO) are taken from [9].

the Table VIII, our DEIO beats the event-only methods (ESVO, ESVO+IMU, and ESIO) by large margins on all sequences (at least 66.7% lower RMSE). Fig. 4 presents a qualitative comparison of the estimated trajectories of our DEIO and these stereo event-based baselines. The results from our DEIO align more closely with the ground truth, even though our employ the monocular setup while the others with stereo setup. This proves that the DEIO can obtain comparable scale estimation to these stereo setup and shows better state estimation result. What's more, as can be seen from the results, the purely event-based odometry (ESVO) exhibits the most significant drift. Although the other stereo event+IMU fusion methods do not perform as well as ours, they maintain minimal drift, emphasizing the

TABLE VII. Accuracy Comparison of Our DEIO with Other Image/Event-based Baseline in MVSEC [48]

Methods	Modality	Flying_1	Flying_2	Flying_3	Flying_4	Average
ORB-SLAM3 [42]	Stereo F+I	5.31	5.65	2.90	6.99	5.21
VINS-Fusion [43]	Stereo F+I	1.50	6.98	0.73	3.62	3.21
EVO [1]	E	5.09	failed	2.58	failed	3.84
ESVO [2]	Stereo E	4.00	3.66	1.71	failed	3.12
Ultimate-SLAM [3]	E+F+I	failed	failed	failed	2.77	2.77
PL-EVIO [4]	E+F+I	1.35	1.00	0.64	5.31	2.08
ESVIO [16]	Stereo E+F+I	0.94	1.00	0.47	5.55	1.99
DPVO [9]	F	0.16	0.15	0.08	0.30	0.17
DBA-Fusion [29]	F+I	2.20	failed	failed	failed	2.20
DEVO [9]	E	0.26	0.32	0.19	1.08	0.46
$DVIO^{\dagger}$	F+I	0.20	0.28	0.16	0.94	0.40
DEIO	E+I	0.24	0.21	0.12	0.78	0.34

Unit: MPE(%); Aligning the whole ground truth trajectory with estimated poses; The Baseline numbers (DPVO, DEVO) are taken from [9].

TABLE VIII. Accuracy Comparison of Our DEIO with Stereo Event-based Methods in DSEC [49]

Methods	Modality		Average				
Wethods	Wiodanty	a	b	c	d	e	Average
ESVO [2]	Stereo E	371.1	116.6	1357.1	2676.6	794.9	1032.9
ESVO+IMU [50]	Stereo E+I	105.0	66.7	637.9	699.8	130.3	527.9
ES-PTAM [46]	Stereo E	131.62	29.02	1184.37	1053.87	75.9	494.9
ESIO [16]	Stereo E+I	543.5	295.1	896.2	2977.0	2326.4	1587.8
ESVIO [16]	Stereo E+F+I	371.2	445.8	1892.7	921.7	352.0	596.9
DEIO	E+I	80.6	35.4	413.8	207.6	86.1	164.5

Unit: ATE/RMSE(cm); Aligning the whole ground truth trajectory with estimated poses; Baseline numbers (ESVO and ESVO+IMU) are taken from [50], and ES-PTAM is sourced from [46].

importance of complementarity between visual events and IMU sensors.

## B. Test on Night Driving Scenarios

Driving scenarios, especially in nighttime driving environments, pose challenges for event-based state estimation because forward motion typically generates much fewer events events in the center of the image compared to the surrounding area, while the apparent motion at the center of the image is minimal. What's more, the movement of vehicles, such as sharp turns, sudden stops, and other abrupt movements can further complicate the event-based estimator. In this section, we selected the *Dense\_street\_night\_easy\_a* 

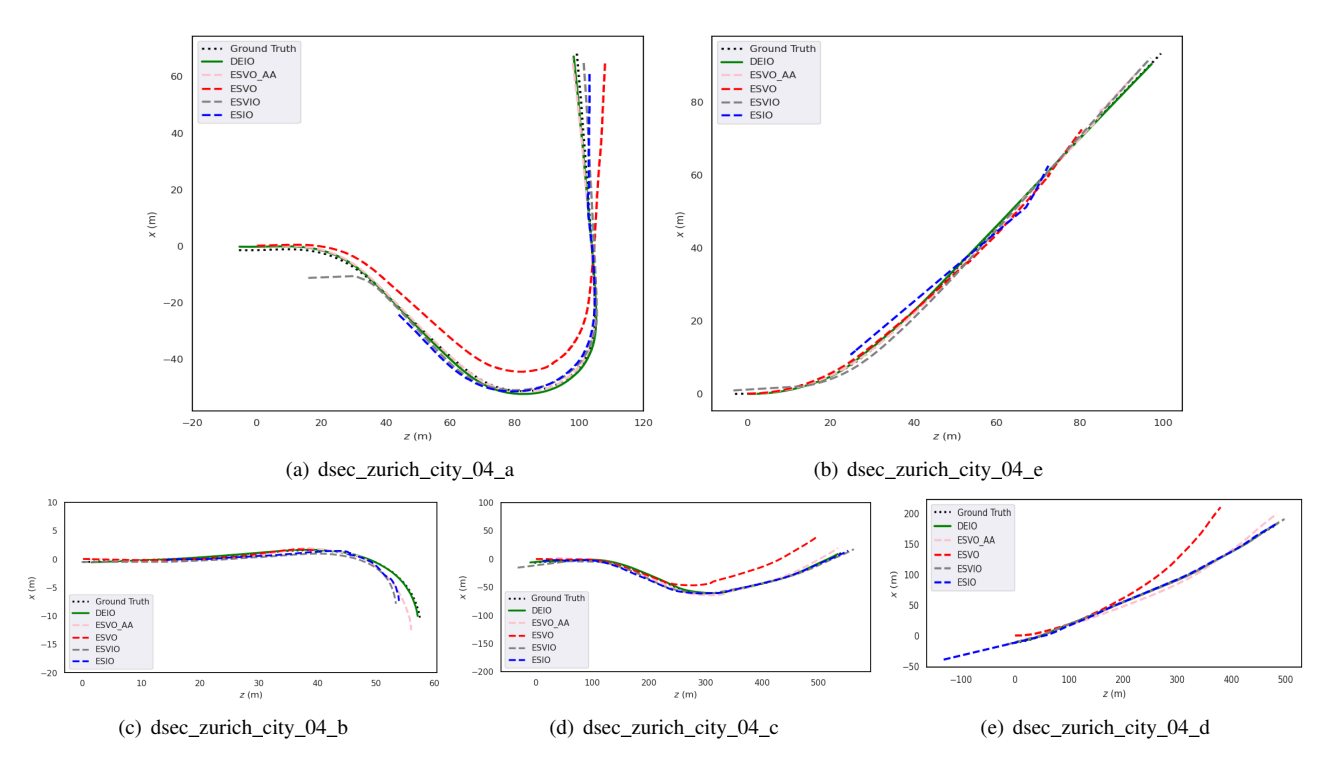


Fig. 4. Comparison of Estimated trajectories on the DSEC dataset [49].

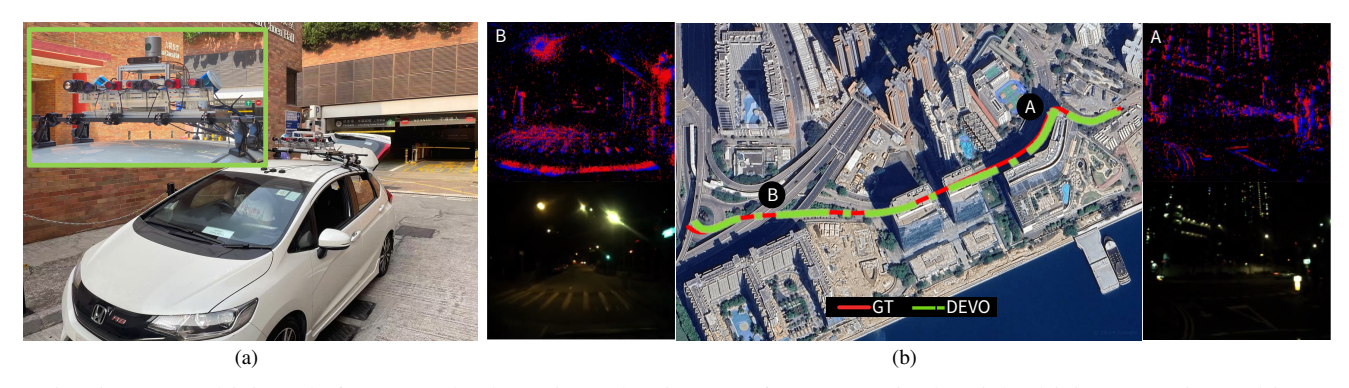


Fig. 5. (a) Our driving platform [8]; (b)The estimated trajectory of our DEIO in the night driving scenarios and its comparison against the GNSS-INS-RTK as ground-truth; The image frame is for visualization-only;

sequences of the ECMD dataset [8], which feature numerous flashing lights from vehicles, street signs and the surrounding buildings, as well as many moving vehicles, making eventbased SLAM more difficult. This dataset were recorded with two pairs of stereo event cameras  $(640 \times 480 \text{ and } 346 \times 260)$ on a car driven through various road conditions such as streets, highways, road, tunnels in Hong Kong. Our DEIO runs on the event from the DAVIS346 and the IMU sensor, while image frame output of the DAVIS346 is only used for illustration purposes. Fig. 5(b) shows small drift with 4.7m error of our estimated trajectory on the 620m drive. To the best of our knowledge, we present the first results on pose tracking for night driving scenarios using event and IMU odometry. The earliest attempt in this area was ESVIO [8], [16], which utilized a combination of stereo events, images, and IMU data, while the DEIO is monocular setup.

# C. Test on Dark Quadrotor-Flight

In this section, we evaluate our DEIO in a dark quadrotor flight experiment. The quadrotor is commanded to track a circle pattern with 1.5m in radius and 1.8m in height, shown in Fig. 6(b). The illuminance in the environment is quite low, resulting in minimal visual information captured by the onboard camera (Fig. 6(a)). The total length of the trajectory is 60.7m, with a MPE of 0.15 and an average pose tracking error of 9cm. We further illustrate the estimated trajectories (translation and rotation) of our DEIO against the ground truth, as well as their corresponding errors (Fig. 6(c)). The translation errors in the X, Y, and Z dimensions are all within 0.5m, while the rotation error of the Roll and Pitch dimensions are within 6°, and the one in the Yaw dimension is within 10°. To the best of our knowledge, this is also the first implementation of event-inertial odometry for pose tracking in dark flight environments, while the

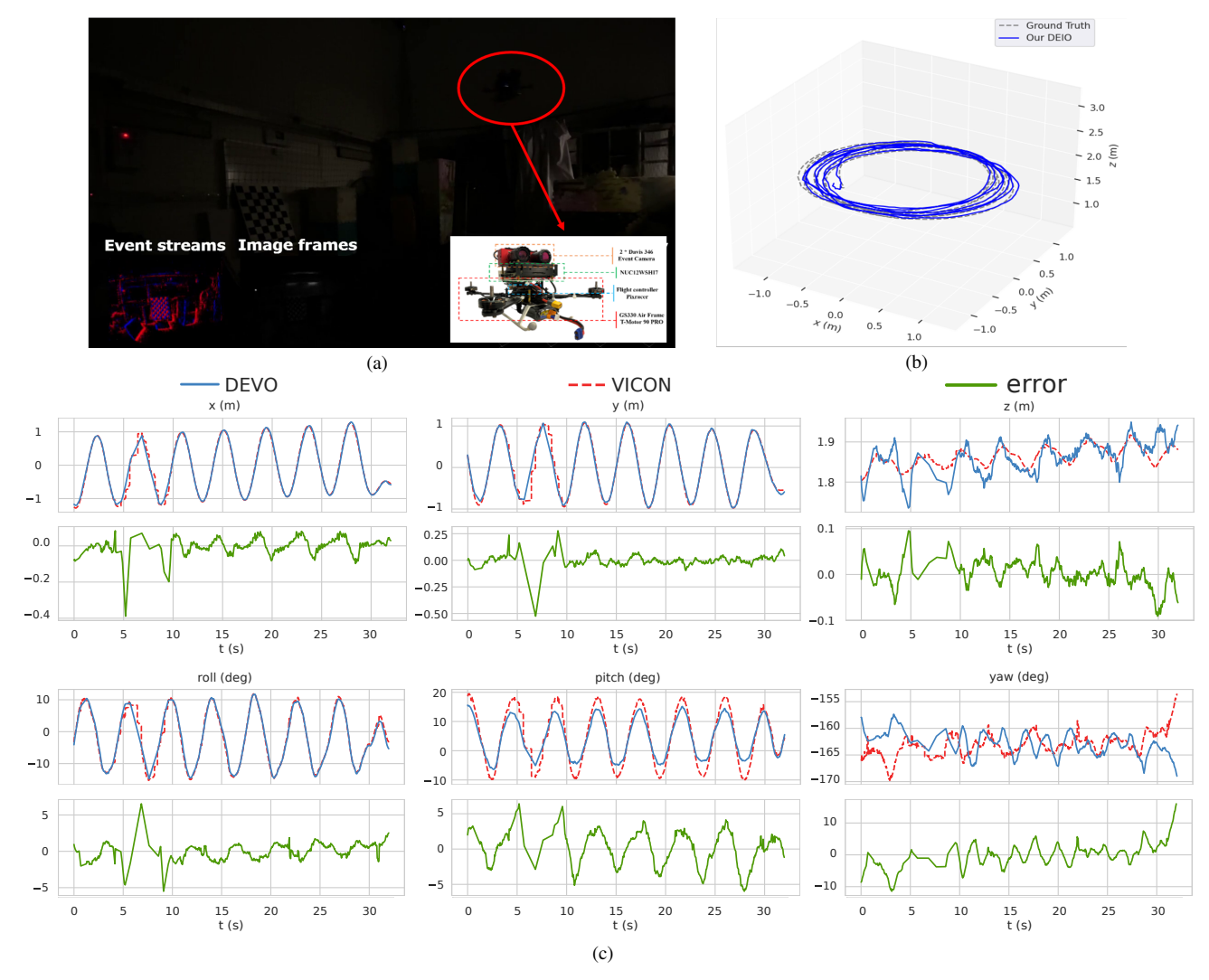


Fig. 6. (a) Our quadrotor platform [16]; (b) The estimated trajectory of our DEIO in the quadrotor flight and its comparison against the ground truth; (c) The position, orientation, and the corresponding errors of DEIO in quadrotor flight compared with the ground truth from VICON.

previous works [3], [16] reply on the image-aided event-inertial estimators.

# D. Ablation Study

## V. CONCLUSION

In this paper, we proposes DEIO which is a Learning-based event-inertial odometry that tightly integrates the deep event-based bundle adjustment with IMU in sliding window graph-based optimization. Evaluation on nine challenging event-based benchmarks demonstrates the superior performance of DEIO compared to image-based and event-based baselines. We show that learning-optimization-combined framework for SLAM is a promising direction. In future work, we might further explore the IMU-bias online learning and loop closure mechanisms for learning-based event-SLAM with global BA to enhance the robustness and efficiency of the system.

## REFERENCES

- [1] H. Rebecq, T. Horstschäfer, G. Gallego, and D. Scaramuzza, "Evo: A geometric approach to event-based 6-dof parallel tracking and mapping in real time," *IEEE Robotics and Automation Letters*, vol. 2, no. 2, pp. 593–600, 2016.
- [2] Y. Zhou, G. Gallego, and S. Shen, "Event-based stereo visual odometry," *IEEE Transactions on Robotics*, vol. 37, no. 5, pp. 1433–1450, 2021.
- [3] A. R. Vidal, H. Rebecq, T. Horstschaefer, and D. Scaramuzza, "Ultimate slam? combining events, images, and imu for robust visual slam in hdr and high-speed scenarios," *IEEE Robotics and Automation Letters*, vol. 3, no. 2, pp. 994–1001, 2018.
- [4] W. Guan, P. Chen, Y. Xie, and P. Lu, "Pl-evio: Robust monocular event-based visual inertial odometry with point and line features," *IEEE Transactions on Automation Science and Engineering*, 2023.
- [5] J. Hidalgo-Carrió, G. Gallego, and D. Scaramuzza, "Event-aided direct sparse odometry," in *Proceedings of the IEEE/CVF Conference* on Computer Vision and Pattern Recognition, 2022, pp. 5781–5790.
- [6] Y.-F. Zuo, J. Yang, J. Chen, X. Wang, Y. Wang, and L. Kneip, "Devo: Depth-event camera visual odometry in challenging conditions," in 2022 International Conference on Robotics and Automation (ICRA). IEEE, 2022, pp. 2179–2185.
- [7] M. Cui, Y. Zhu, Y. Liu, Y. Liu, G. Chen, and K. Huang, "Dense depthmap estimation based on fusion of event camera and sparse lidar,"

- *IEEE Transactions on Instrumentation and Measurement*, vol. 71, pp. 1–11, 2022
- [8] P. Chen, W. Guan, F. Huang, Y. Zhong, W. Wen, L.-T. Hsu, and P. Lu, "Ecmd: An event-centric multisensory driving dataset for slam," *IEEE Transactions on Intelligent Vehicles*, 2023.
- [9] S. Klenk, M. Motzet, L. Koestler, and D. Cremers, "Deep event visual odometry," in 2024 International Conference on 3D Vision (3DV). IEEE, 2024, pp. 739–749.
- [10] W. Guan and P. Lu, "Monocular event visual inertial odometry based on event-corner using sliding windows graph-based optimization," in 2022 IEEE/RSJ International Conference on Intelligent Robots and Systems (IROS). IEEE, 2022, pp. 2438–2445.
- [11] H. Kim, S. Leutenegger, and A. J. Davison, "Real-time 3d reconstruction and 6-dof tracking with an event camera," in *European Conference on Computer Vision*. Springer, 2016, pp. 349–364.
- [12] H. Rebecq, G. Gallego, E. Mueggler, and D. Scaramuzza, "Emvs: Event-based multi-view stereo—3d reconstruction with an event camera in real-time," *International Journal of Computer Vision*, vol. 126, no. 12, pp. 1394–1414, 2018.
- [13] G. Gallego, J. E. Lund, E. Mueggler, H. Rebecq, T. Delbruck, and D. Scaramuzza, "Event-based, 6-dof camera tracking from photometric depth maps," *IEEE transactions on pattern analysis and machine* intelligence, vol. 40, no. 10, pp. 2402–2412, 2017.
- [14] S. Guo and G. Gallego, "Cmax-slam: Event-based rotational-motion bundle adjustment and slam system using contrast maximization," *IEEE Transactions on Robotics*, 2024.
- [15] W. Chamorro, J. Solà, and J. Andrade-Cetto, "Event-imu fusion strategies for faster-than-imu estimation throughput," in *Proceedings of the IEEE/CVF Conference on Computer Vision and Pattern Recognition*, 2023, pp. 3975–3982.
- [16] P. Chen, W. Guan, and P. Lu, "Esvio: Event-based stereo visual inertial odometry," *IEEE Robotics and Automation Letters*, vol. 8, no. 6, pp. 3661–3668, 2023.
- [17] W. Guan, P. Chen, H. Zhao, Y. Wang, and P. Lu, "Evi-sam: Robust, real-time, tightly-coupled event-visual-inertial state estimation and 3d dense mapping," *Advanced Intelligent Systems*, 2024.
- [18] A. Z. Zhu, L. Yuan, K. Chaney, and K. Daniilidis, "Unsupervised event-based learning of optical flow, depth, and egomotion," in Proceedings of the IEEE/CVF Conference on Computer Vision and Pattern Recognition, 2019, pp. 989–997.
- [19] J. Hidalgo-Carrió, D. Gehrig, and D. Scaramuzza, "Learning monocular dense depth from events," in 2020 International Conference on 3D Vision (3DV). IEEE, 2020, pp. 534–542.
- [20] D. Gehrig, M. Rüegg, M. Gehrig, J. Hidalgo-Carrió, and D. Scaramuzza, "Combining events and frames using recurrent asynchronous multimodal networks for monocular depth prediction," *IEEE Robotics and Automation Letters*, vol. 6, no. 2, pp. 2822–2829, 2021.
- [21] S. H. Ahmed, H. W. Jang, S. N. Uddin, and Y. J. Jung, "Deep event stereo leveraged by event-to-image translation," in *Proceedings of the* AAAI Conference on Artificial Intelligence, vol. 35, no. 2, 2021, pp. 882–890.
- [22] A. Soliman, F. Bonardi, D. Sidibé, and S. Bouchafa, "Dh-ptam: a deep hybrid stereo events-frames parallel tracking and mapping system," *IEEE Transactions on Intelligent Vehicles*, 2024.
- [23] Z. Teed, L. Lipson, and J. Deng, "Deep patch visual odometry," Advances in Neural Information Processing Systems, vol. 36, 2024.
- [24] R. Pellerito, M. Cannici, D. Gehrig, J. Belhadj, O. Dubois-Matra, M. Casasco, and D. Scaramuzza, "End-to-end learned event-and image-based visual odometry," arXiv preprint arXiv:2309.09947, 2023.
- [25] Z. Teed and J. Deng, "Raft: Recurrent all-pairs field transforms for optical flow," in *Computer Vision–ECCV 2020: 16th European Conference, Glasgow, UK, August 23–28, 2020, Proceedings, Part II* 16. Springer, 2020, pp. 402–419.
- [26] Z. Teed and J. Deng, "Droid-slam: Deep visual slam for monocular, stereo, and rgb-d cameras," Advances in neural information processing systems, vol. 34, pp. 16558–16569, 2021.
- [27] W. Wang, D. Zhu, X. Wang, Y. Hu, Y. Qiu, C. Wang, Y. Hu, A. Kapoor, and S. Scherer, "Tartanair: A dataset to push the limits of visual slam," in 2020 IEEE/RSJ International Conference on Intelligent Robots and Systems (IROS). IEEE, 2020, pp. 4909–4916.
- [28] H. Rebecq, D. Gehrig, and D. Scaramuzza, "Esim: an open event camera simulator," in *Conference on robot learning*. PMLR, 2018, pp. 969–982.

- [29] Y. Zhou, X. Li, S. Li, X. Wang, S. Feng, and Y. Tan, "Dba-fusion: Tightly integrating deep dense visual bundle adjustment with multiple sensors for large-scale localization and mapping," *IEEE Robotics and Automation Letters*, 2024.
- [30] T. Qin, P. Li, and S. Shen, "Vins-mono: A robust and versatile monocular visual-inertial state estimator," *IEEE Transactions on Robotics*, vol. 34, no. 4, pp. 1004–1020, 2018.
- [31] T. Qin and S. Shen, "Robust initialization of monocular visual-inertial estimation on aerial robots," in 2017 IEEE/RSJ International Conference on Intelligent Robots and Systems (IROS). IEEE, 2017, pp. 4225–4232.
- [32] E. Mueggler, H. Rebecq, G. Gallego, T. Delbruck, and D. Scaramuzza, "The event-camera dataset and simulator: Event-based data for pose estimation, visual odometry, and slam," *The International Journal of Robotics Research*, vol. 36, no. 2, pp. 142–149, 2017.
- [33] S. Klenk, J. Chui, N. Demmel, and D. Cremers, "Tum-vie: The tum stereo visual-inertial event dataset," in 2021 IEEE/RSJ International Conference on Intelligent Robots and Systems (IROS). IEEE, 2021, pp. 8601–8608.
- [34] A. Zihao Zhu, N. Atanasov, and K. Daniilidis, "Event-based visual inertial odometry," in *Proceedings of the IEEE Conference on Computer Vision and Pattern Recognition*, 2017, pp. 5391–5399.
- [35] H. Rebecq, T. Horstschaefer, and D. Scaramuzza, "Real-time visual-inertial odometry for event cameras using keyframe-based nonlinear optimization," in *British Machine Vision Conference (BMVC)*, 2017.
- [36] J. H. Jung and C. G. Park, "Constrained filtering-based fusion of images, events, and inertial measurements for pose estimation," in 2020 IEEE International Conference on Robotics and Automation (ICRA). IEEE, 2020, pp. 644–650.
- [37] I. Alzugaray and M. Chli, "Asynchronous multi-hypothesis tracking of features with event cameras," in 2019 International Conference on 3D Vision (3DV). IEEE, 2019, pp. 269–278.
- [38] F. Mahlknecht, D. Gehrig, J. Nash, F. M. Rockenbauer, B. Morrell, J. Delaune, and D. Scaramuzza, "Exploring event camera-based odometry for planetary robots," *IEEE Robotics and Automation Letters (RA-L)*, 2022.
- [39] B. Dai, C. Le Gentil, and T. Vidal-Calleja, "A tightly-coupled eventinertial odometry using exponential decay and linear preintegrated measurements," in 2022 IEEE/RSJ International Conference on Intelligent Robots and Systems (IROS). IEEE, 2022, pp. 9475–9482.
- [40] M. S. Lee, J. H. Jung, Y. J. Kim, and C. G. Park, "Event-and frame-based visual-inertial odometry with adaptive filtering based on 8-dof warping uncertainty," *IEEE Robotics and Automation Letters*, 2023.
- [41] M. Grupp, "evo: Python package for the evaluation of odometry and slam," Note: https://github. com/MichaelGrupp/evo Cited by: Table, vol. 7, 2017.
- [42] C. Campos, R. Elvira, J. J. G. Rodríguez, J. M. Montiel, and J. D. Tardós, "Orb-slam3: An accurate open-source library for visual, visual-inertial, and multimap slam," *IEEE Transactions on Robotics*, vol. 37, no. 6, pp. 1874–1890, 2021.
- [43] T. Qin, J. Pan, S. Cao, and S. Shen, "A general optimization-based framework for local odometry estimation with multiple sensors," arXiv preprint arXiv:1901.03638, 2019.
- [44] J. H. Jung, Y. Choe, and C. G. Park, "Photometric visual-inertial navigation with uncertainty-aware ensembles," *IEEE Transactions on Robotics*, vol. 38, no. 4, pp. 2039–2052, 2022.
- [45] L. Gao, Y. Liang, J. Yang, S. Wu, C. Wang, J. Chen, and L. Kneip, "Vector: A versatile event-centric benchmark for multi-sensor slam," *IEEE Robotics and Automation Letters*, 2022.
- [46] S. Ghosh, V. Cavinato, and G. Gallego, "ES-PTAM: Event-based stereo parallel tracking and mapping," in European Conference on Computer Vision (ECCV) Workshops, 2024.
- [47] J. Delmerico, T. Cieslewski, H. Rebecq, M. Faessler, and D. Scaramuzza, "Are we ready for autonomous drone racing? the uzh-fpv drone racing dataset," in 2019 International Conference on Robotics and Automation (ICRA). IEEE, 2019, pp. 6713–6719.
- [48] A. Z. Zhu, D. Thakur, T. Özaslan, B. Pfrommer, V. Kumar, and K. Daniilidis, "The multivehicle stereo event camera dataset: An event camera dataset for 3d perception," *IEEE Robotics and Automation Letters*, vol. 3, no. 3, pp. 2032–2039, 2018.
- [49] M. Gehrig, W. Aarents, D. Gehrig, and D. Scaramuzza, "Dsec: A stereo event camera dataset for driving scenarios," *IEEE Robotics and Automation Letters*, vol. 6, no. 3, pp. 4947–4954, 2021.
- [50] J. Niu, S. Zhong, and Y. Zhou, "Imu-aided event-based stereo visual odometry," arXiv preprint arXiv:2405.04071, 2024.